Image quality evaluation of small FOV and large FOV CBCT devices for oral and maxillofacial radiology

Jean-Philippe Dillenseger, Catherine-Isabelle Gros, Amira Sayeh, Johary Rasamimanana, Fabrice Lawniczak, Jean-Marie Le Minor, Jean-François Matern, André Constantinesco, Fabien Bornert, Philippe Choquet

Dentomaxillofacial Radiology (2016) 45, 20160285

birpublications.org/dmfr

TECHNICAL REPORT

Image quality evaluation of small FOV and large FOV CBCT devices for oral and maxillofacial radiology

[1,2,3]Jean-Philippe Dillenseger, [3,4]Catherine-Isabelle Gros, [4]Amira Sayeh, [5]Johary Rasamimanana, [5]Fabrice Lawniczak, [2,3,6]Jean-Marie Leminor, [1]Jean-François Matern, [1]André Constantinesco, [3,4]Fabien Bornert and [1,2,3]Philippe Choquet

[1]Imagerie Préclinique, Pôle d'imagerie, Hôpitaux Universitaires de Strasbourg, Strasbourg, France; [2]Icube, équipe MMB, CNRS, Université de Strasbourg, Strasbourg, France; [3]Fédération de Médecine Translationnelle de Strasbourg, Faculté de Médecine, Université de Strasbourg, Strasbourg, France; [4]Faculté de Chirurgie Dentaire, Université de Strasbourg, Strasbourg, France; [5]Icube, équipe Mécaflu, Université de Strasbourg, Strasbourg, France; [6]Institut d'Anatomie Normale, Université de Strasbourg, Strasbourg, France

Objectives: Quantitative and qualitative image quality evaluation of two different dental CBCT scanners.
Methods: Two CBCT systems were evaluated in this study: one small field-of-view (FOV) (50-mm diameter) system that also allows two-dimensional (2D) dental panoramic imaging and one large FOV CBCT system (60–180-mm diameter). These devices were all tested with installed acquisition default modes and proprietary reconstruction software, enabling high-resolution bone imaging. Quantitative analyses were carried out to measure spatial resolution, linearity and homogeneity. Small-size phantoms and a human dry skull were used to evaluate intrinsic performances. Visual qualitative analyses of specific anatomical parts were blindly performed by 10 operators.
Results: Concerning spatial resolution, small-voxel size protocols provide equivalent results on the two apparatus. In terms of linearity, all systems are highly linear ($0.98 < r^2 < 0.99$) over the range of signal intensities encountered. Our results, coming from either phantoms or the dry skull, demonstrate that the small FOV CBCT suffers from a lack of homogeneity.
Conclusions: For limited oral and maxillofacial volume imaging (diameter < 50 mm), the polyvalent small FOV CBCT (2D and three-dimensional imaging) system used in this study could reach performances similar to those of the large FOV CBCT.
Dentomaxillofacial Radiology (2016) **45**, 20160285. doi: 10.1259/dmfr.20160285

Cite this article as: Dillenseger J-P, Gros C-I, Sayeh A, Rasamimanana J, Lawniczak F, Leminor J-M, et al. Image quality evaluation of small FOV and large FOV CBCT devices for oral and maxillofacial radiology. *Dentomaxillofac Radiol* 2016; **45**: 20160285.

Keywords: CBCT; bone imaging; dental imaging; quantitative evaluation; radiologic phantoms

Introduction

Diagnosis of thin dentomaxillary lesions requires high-definition bone imaging. Nowadays, X-ray CT is the best available technique for studying bone and dental structures. Clinical applications concerning the oral and maxillofacial (OMF) region need not only high resolution (*e.g.* dentoalveolar traumatology), but also enough contrast (*e.g.* detection of radiolucent findings before they could be visualized on conventional radiographs). Since early 2000,[1,2] specific CT architectures were designed for high-resolution skull bone imaging using a flat-panel detector called CBCT. Several designs of CBCT exist which could be separated into two groups:[3]

Correspondence to: Mr Jean-Philippe Dillenseger. E-mail: jp.dillenseger@unistra.fr
Received 6 July 2016; revised 29 July 2016; accepted 30 August 2016

Table 1 Systems characteristics and protocol parameters

Manufacturer	*Newtom™ DR srl*				*Planmeca*			
Model	VGi				Promax 3D classic			
Detectors characteristics	Amorphous silicon FPD : 20 × 25 cm				Amorphous silicon FPD : 13.5 × 13.5 cm			
Focal spot dimension (mm^2)	0.3 × 0.3				0.5 × 0.5			
Protocol number	1	2	3	4	5	6	7	8
Manufacturer protocol name	High Res Zoom	Hi Res	Zoom	Full	Endo (M)	Hi Res (M)	Normal (M)	Low dose (M)
Programmed tube potential (kV)	110				90			
Programmed tube current (mA)	Auto				14	12.5	11	4.5
Total filtration	12 mmAl at 75 kV (equivalent)				2.5 mmAl + 0.5 mmCu			
Emission mode	Pulsed				Pulsed			
FOV diameter (mm)	60	80	150	180	50			
Z-axis collimation (mm)	60	80	120	150	50		80	
Reconstructed voxel size (μm^3)	75 × 75 × 75	150 × 150 × 150	250 × 250 × 250	300 × 300 × 300	75 × 75 × 75	100 × 100 × 100	200 × 200 × 200	400 × 400 × 400
Rotation angle (°)/number of projections	360/360				220/220			
Rotation duration (s)	27		20		35	35	30	30
2D dental panoramic imaging	Available				N/A			

2D, two-dimensional; FPD, flat-panel detector; FOV, field of view.

– Small field-of-view (FOV) CBCT that could acquire only a limited volume of the OMF region (diameter < 50 mm), but could also achieve two-dimensional (2D) dental panoramic imaging. In general, these kinds of architecture are low-cost systems.

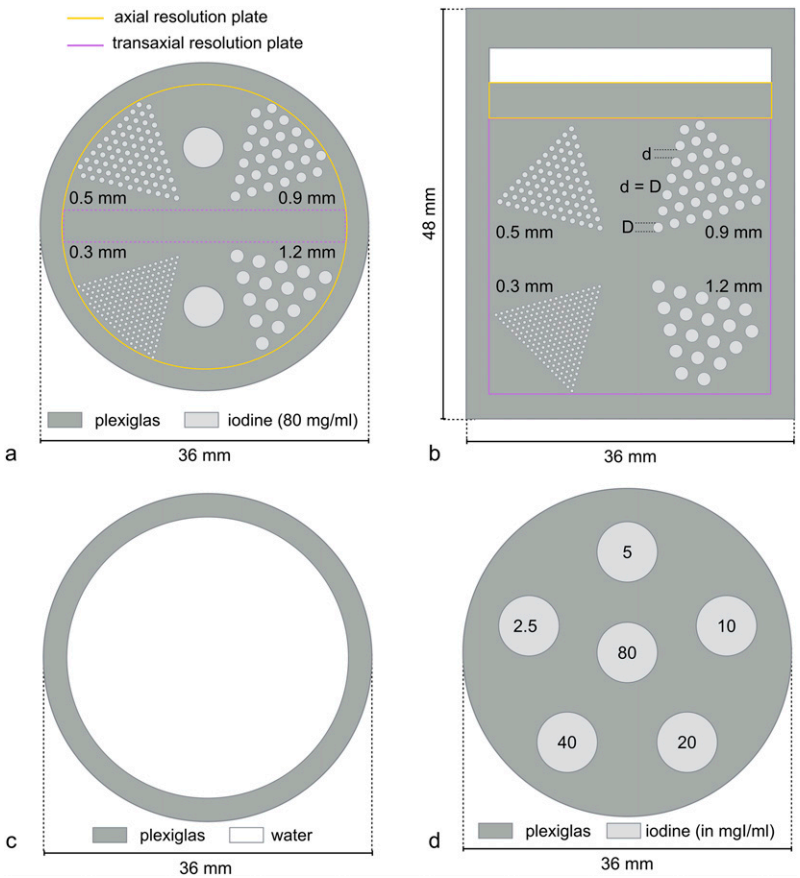

Figure 1 Superior (a) and lateral (b) views of the resolution phantom: Jaszczak areas (diameter D = distance d) allow evaluation of axial resolution (a) and transaxial resolution (b). Superior views of the homogeneity phantom (c) and the linearity phantom (d) with iodine concentration listed in milligram per millilitre ($mg.ml^{-1}$).

Table 2 Phantom analysis scoring

Phantom analysis scale	*Score*					
Jaszczak 1200 μm	Not visible	0	Lightly visible	1	Clearly visible	2
Jaszczak 900 μm	Not visible	0	Lightly visible	1	Clearly visible	2
Jaszczak 500 μm	Not visible	0	Lightly visible	1	Clearly visible	2
Jaszczak 300 μm	Not visible	0	Lightly visible	1	Clearly visible	2
Blurring and artefacts	Detrimental	0	Troublesome	1	Not visible	2

– Large FOV CBCT, which is able to acquire complete OMF region (diameter > 16 cm).

We compare in this study two CBCT, one small FOV and one large FOV, from two different manufacturers, which have been installed in our university hospital since 2014. The purpose of this study was to compare performances, on a limited volume of the OMF region, in terms of image quality, between a small FOV CBCT and a large FOV CBCT. We measured linearity, geometric accuracy, homogeneity and spatial resolution with phantoms presenting patterns (*e.g.* spatial resolution pattern) that could be contained in small FOV acquisitions (FOV <60 mm). We choose small-size phantoms (diameter: 36 mm, length: 48 mm) to limit the Compton effect, in order to be in the most favourable conditions: it allows to reach the intrinsic performances of the instruments. For the same reason, and to complete the quantitative analysis, a human dry skull was scanned in the same conditions.[4] Each CBCT system was tested with default manufacturer protocols used in our clinical routine. Qualitative and practical aspects concerning these two apparatus were also discussed.

Methods and materials

CT systems and acquisition protocols

CBCT instruments were a Newtom™ VGi (QR s.r.l, Verona, Italy) and a Planmeca Promax® 3D (Planmeca, Roselle, IL). The Newtom™ VGi CBCT allows complete OMF region exploration (60 mm < FOV < 180 mm), whereas the Planmeca Promax 3D is a multifunctional device allowing small FOV CBCT (FOV: 50 mm) acquisitions but also 2D dental panoramic imaging. All apparatus were up to date in terms of hardware and software at the time of the study. Reconstructions were carried out using the proprietary software. The characteristics of the CBCT systems and protocol acquisitions are summarized in Table 1. Each acquisition has been numbered (from 1 to 8). This identification number will be used in the following for further reference. For each CBCT scanner, we applied four proposed standard protocols, covering several voxel sizes.

Phantoms

We designed three different plexiglass phantoms, to evaluate each particular aspect of image quality (*e.g.* resolution, linearity, uniformity and noise). All phantoms have an outer diameter of 36 mm for a total length of 48 mm (Figure 1). These dimensions are adapted for small FOV (Table1).

Resolution phantom

The resolution phantom [Figure 1(a,b)] allows a visual qualitative measurement of the spatial resolution of the system. Plexiglass plates of 4-mm thickness were placed orthogonally and named axial and transaxial resolution plates, respectively. Each plate is divided into four areas, riddled with wells following Jaszczak patterns[5] with diameters of 0.3, 0.5, 0.9 and 1.2 mm corresponding to 1.67, 1.0, 0.55 and 0.41 lp mm^{-1}, respectively. The Jaszczak patterns were filled with an iodine solution of Visipaque™ 320 (GE Healthcare, Little Chalfont, UK) diluted at 80 mgI ml^{-1}. The standard deviations (SDs) of voxel values were measured in four cylindrical volumes of interest (diameter: 3 mm; thickness: 1 mm) placed on each Jaszczak area (top, bottom, left and right). They were corrected by the SD of a uniform region of the phantom. For quantitative spatial resolution analysis, axial and transaxial modulation transfer function (MTF) values were calculated for each Jaszczak area using the average SD and the mean absolute difference CT values, measured for iodine and plexiglass.[6,7] The reference value (MTF100) was determined from the CT number for pure iodine (CT_{iodine}) and plexiglass (CT_{plexi}), according to the Formula (1):

$$MTF100 = \frac{|CT_{iodine} - CT_{plexi}|}{2}. \quad (1)$$

A subjective blinded visual analysis was conducted by 10 trained CT users (3 radiologists, 4 dental surgeons and 3 technologists) to qualitatively classify the different acquisitions. This analysis was performed using the free software OsiriX (http://www.osirix-viewer.com).[8] Observers had access to all tools offered by the software (*e.g.* windowing, magnification) and could use them,

Table 3 Human skull analysis scoring

Skull analysis scale	*Score*					
Dental and peridental	Low quality	0	Convenient	1	High quality	2
Alveolar bone	Low quality	0	Convenient	1	High quality	2
Blurring and artefacts	Detrimental	0	Troublesome	1	Non visible	2

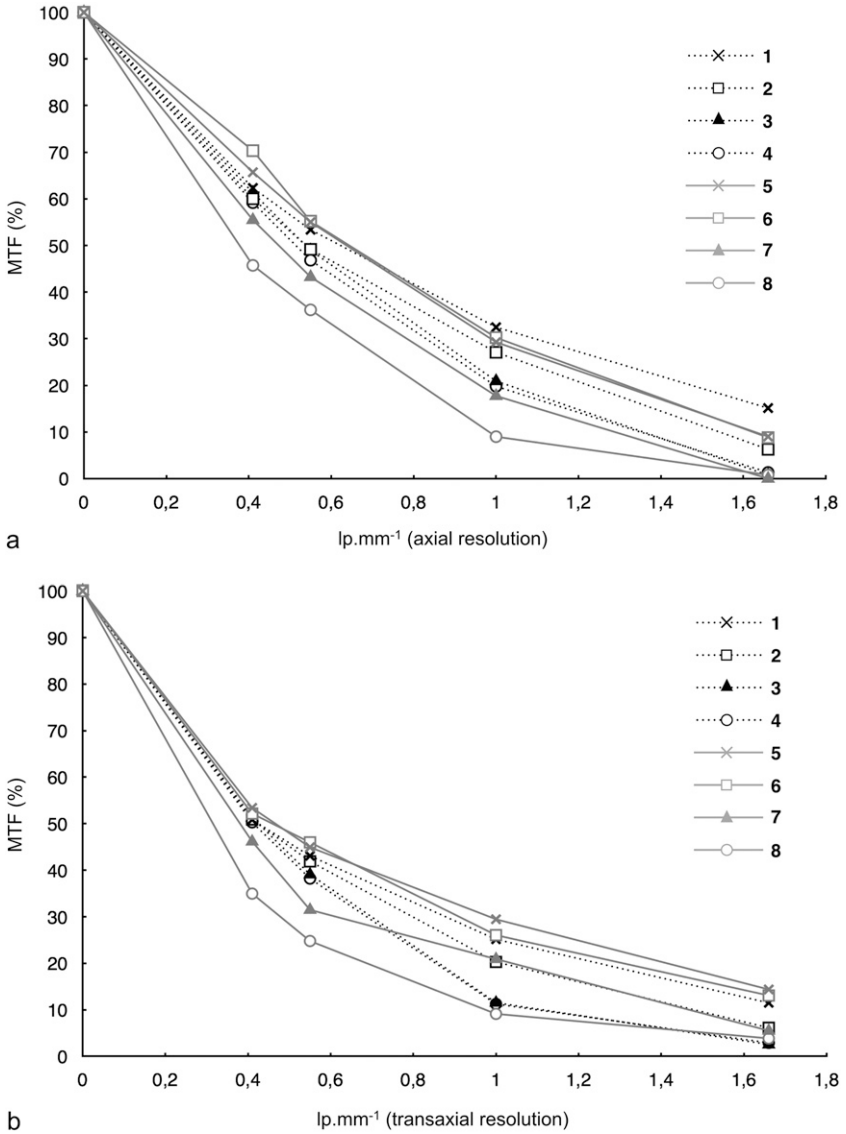

Figure 2 Modulation transfer function (MTF) of each protocol (from 1 to 8; Table 1) measured from the Jaszczak resolution plates—axial resolution (a) and transaxial resolution (b). lp.mm^{-1}, line pairs per millimetre.

following their habits. For each acquisition, a semi-quantitative visual scale using three subscores that evaluated spatial resolution, blurring and image artefacts was applied (Table 2). The different acquisitions were ranked from these results.

Uniformity phantom

The uniformity phantom is made of a plexiglass cylinder (diameter: 36 mm; length: 48 mm) filled with water. Four peripheral regions of interest (ROIs) and one central cylindrical ROI (diameter: 3 mm; thickness: 1 mm) were drawn on the uniformity phantom image in order to quantitatively assess variation in signal intensity from the centre to the periphery. Average differences in signal intensity between the peripheral and the central regions as well as average SD measured in the five ROIs were used to evaluate the uniformity. The total measured noise can be considered as a quadrature summation of photon noise and system noise.[6] Contrast-to-noise ratio (CNR) was also measured, using OsiriX,[8] between water and air,[9] using the mean CT unit value and the mean SD from five ROIs (diameter: 3 mm; thickness: 1 mm) drawn on the uniformity phantom section as well as in air, according to the Formula (2):

$$\mathrm{CNR} = \frac{|\mathrm{MCT}_{\mathrm{water}} - \mathrm{MCT}_{\mathrm{air}}|}{\sqrt{\mathrm{SD}_{\mathrm{water}}{}^2 + \mathrm{SD}_{\mathrm{air}}{}^2}}. \qquad (2)$$

Linearity phantom

Linearity of the system was determined by the linearity phantom, which consists in plexiglass cylinder riddled with wells of increasing iodine concentrations of 2.5, 5, 10, 20, 40 and 80 mg ml^{-1}. Mean signal intensity and

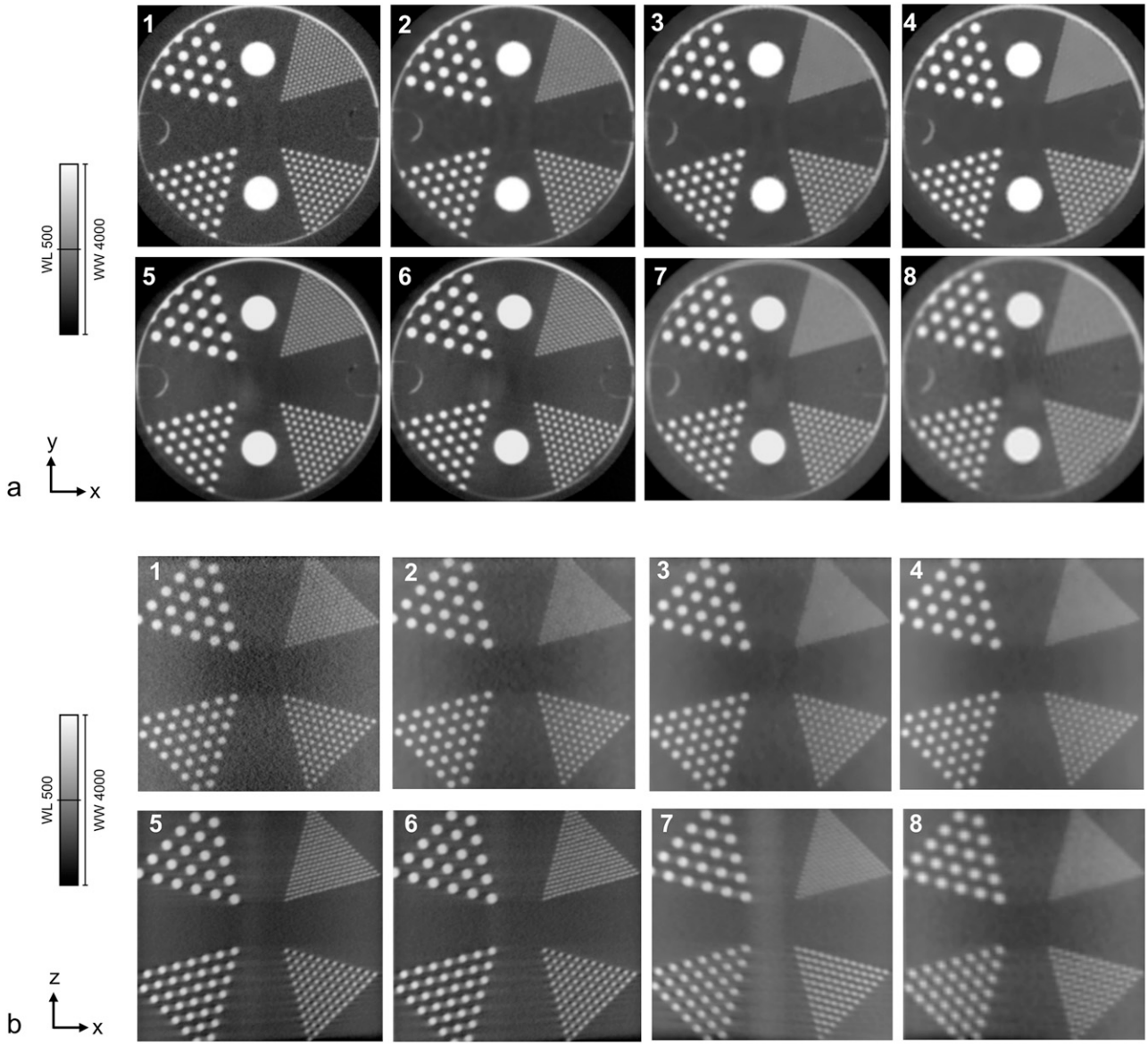

Figure 3 Slices through the axial (a) and transaxial (b) resolution plates for different protocols (1–8; Table 1); window level (WL): 500; window width (WW): 4000.

SD (CT values) for each iodine concentration was measured in cylindrical volumes of interest (diameter: 3 mm; thickness: 1 mm) placed manually at the centre of each well. The relationship between signal intensity and iodine concentration was determined by linear regression analysis (Microsoft Excel®; Redmond, WA).

Human skull bone analysis

A human dry skull was loaned from the collection of the Institute of Normal Anatomy of the Strasbourg Faculty of Medicine in order to test different protocols on a real bone architecture. A blind visual analysis was conducted by 10 different trained CT users (3 radiologists, 4 dental surgeons and 3 technologists) for classifying the different acquisitions. In order to be comparable over the different systems, the same dental region was scanned. For each acquisition, a semi-quantitative visual scale using three subscores that evaluated anatomical structures, blurring and image artefacts was applied (Table 3). The scores were adjusted to 10 and

Table 4 Phantom results

	Phantom axial slices		*Phantom transaxial slices*	
Rank	*Score*	*Acquisition number*	*Score*	*Acquisition number*
1	9.0	1	8.2	1
2	8.3	5	6.6	6
3	8.1	6	6.4	5
4	7.9	2	6.3	2
5	5.7	3	4.8	3
6	5.2	4	4.3	7
7	4	7	4.0	4
8	3.2	8	2.6	8

Table 5 Human skull scoring results

	Dental and peridental		*Alveolar bone*		*Blurring and artefacts*		*Final scoring and ranking*			
	Axial slices	*Transaxial slices*	*Axial slices*	*Transaxial slices*	*Axial slices*	*Transaxial slices*	*Axial slices*		*Transaxial slices*	
Rank	*Acquisition number*	*Acquisition number*	*Acquisition number*	*Acquisition number*	*Acquisition number*	*Acquisition number*	*Score*	*Acquisition number*	*Score*	*Acquisition number*
1	5	5	6	5	2	5	5.3	5	5.2	5
2	6	6	5	6	3	6	5.1	6	4.8	6
3	2	1	1	1	1	2	4.0	1	4.3	1
4	1	2	7	7	6	1	3.9	2	3.6	2
5	7	3	2	2	5	7	3.3	3	3.1	7
6	3	7	3	3	4	3	3.2	4	2.7	3
7	4	4	4	4	7	4	2.6	7	2.3	4
8	8	8	8	8	8	8	1.6	8	1.2	8

the different acquisitions were ranked from these results. Axial, coronal and sagittal planes were evaluated. This blind analysis was performed using the free software OsiriX (http://www.osirix-viewer.com).[8] Observers had access to all tools offered by the software (*e.g.* windowing, magnification) for phantom image evaluation.

Results

Spatial resolution

The in-plane MTF of each system was based on the analysis of the reconstructed images of axial and transaxial resolution plates. For quantitative analysis, MTFs at 1.67, 1, 0.55 and 0.41 lp mm^{-1} of each acquisition are summarized in Figure 2.

The visual qualitative axial and transaxial analyses allowed the visualization of the 1.2-, 0.9- and 0.5-mm Jaszczak areas for each acquisition protocol. The 0.3-mm area was seen in Acquisitions 1, 2, 5 and 6 for the axial plate [Figure 3(a)] and in Acquisitions 1, 5 and 6 for the transaxial plate [Figure 3(b)]. Scores and ranking issued from the different acquisitions are given in Table 4. These rankings match the results observed quantitatively (Figure 2) and place systematically Acquisitions 1, 5 and 6 at the head of the ranking (Table 4).

Linearity

The linearity of the system was determined using the measured CT number in iodine solutions at various concentrations [Figure 1(d)]. Linear correlation coefficients r^2 between measured CT number and iodine concentration are given in Table 5. The r^2 correlation coefficient value is comprised between 0.98 and 0.99, which shows that all systems are highly linear over the range of signal intensities encountered.

Uniformity

Uniformity of the system signal response was measured on the uniformity phantom filled with water [Figure 1 (c)]. CNR and the average difference in signal intensity values between peripheral and central regions are reported in Table 6. Radial signal profiles of the uniformity section illustrate this point (Figure 4).

Acquisitions 5 and 6 generate consequent non-uniform results and Acquisitions 1, 5 and 6 present high noise level and low CNR (Table 5 and Figure 4). In general, we note that in Protocols 5–8, the uniformity (in CT value) was higher than the noise (in CT value) (Table 5). It means that the Planmeca CBCT (Protocols 5–8) provides less homogeneous images than the Newtom™ system (Protocols 1–4) (Table 5 and Figure 4).

Human skull bone analysis

Figure 5 shows an axial slice at the same position of the dental region obtained with each protocol (1–8; Table 1). Figure 6(a,d) present sagittal and coronal slices through the dental region, respectively (1–8; Table 1). Scores and ranking issued from these different anatomical regions are given in Table 4.

The trained users stated that Acquisitions 1, 2, 5 and 6 stand out from the others by systematically taking the lead of the ranking for axial and transaxial planes. Acquisition 8 takes systematically the end of the ranking; the ranking of other acquisitions (3, 4 and 7) varies considerably (Table 5).

Table 6 Linearity and homogeneity results of each protocol (1–8; Table 1)

Acquisition number	*1*	*2*	*3*	*4*	*5*	*6*	*7*	*8*
Linearity								
r^2	0.9931	0.9893	0.9924	0.9912	0.9825	0.9854	0.9878	0.9823
Homogeneity								
Uniformity in CT value (SD)	8.4 (6.4)	6.1 (5.4)	6.5 (3.5)	3.5 (2.5)	119.5 (14.1)	132 (16.0)	15.9 (10.2)	16.6 (3.2)
Noise in CT value (SD)	42.8 (2.6)	11.8 (1.3)	5.8 (1.5)	7.4 (1.3)	28.1 (7.8)	29.2 (7.4)	8.9 (0.8)	14.3 (2.1)
CNR	17	69	141	109	20	19	79	50

CNR, contrast-to-noise ratio; SD, standard deviation.

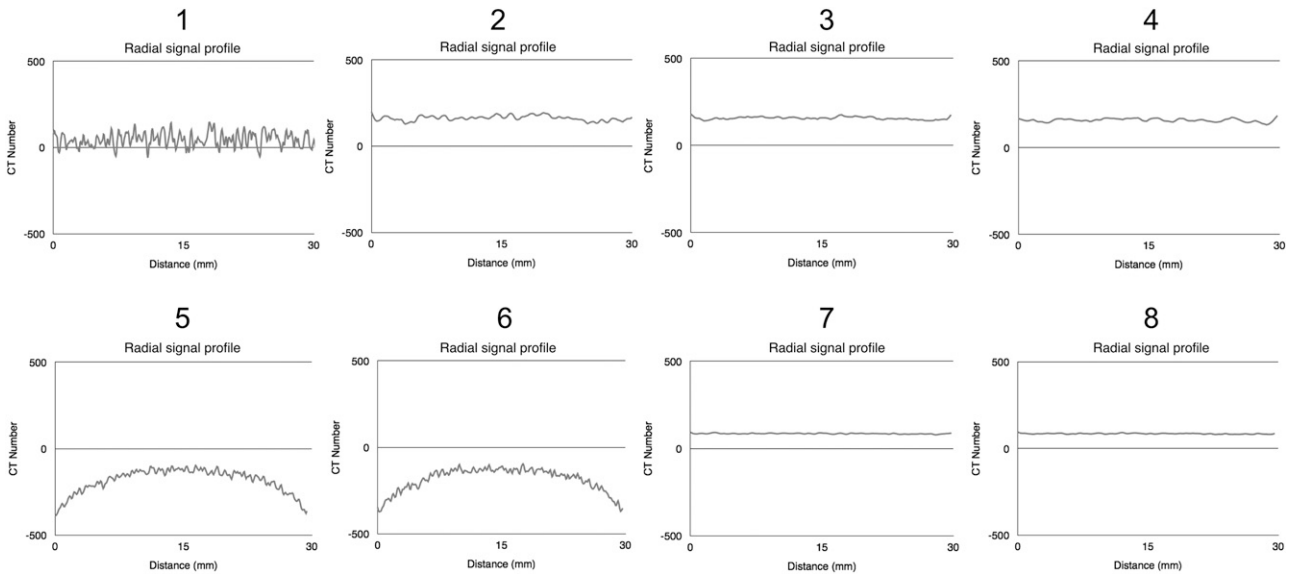

Figure 4 Radial signal profiles of the uniformity phantom for each protocol (1–8; Table 1).

Discussion

This study compares different protocols between two recent but different CBCT systems. The Newtom™ VGi apparatus is a large FOV dentomaxillary dedicated CBCT system and the Planmeca Promax is a multifunctional apparatus which is able to acquire 2D dental panoramic imaging as well as small FOV CBCT for dental imaging (Table 1). To our knowledge, our work is the first study that compares intrinsic performances of these two kinds of CBCT apparatus.

Phantom and dry skull analysis

Spatial resolution is a complex issue that depends on both detector characteristics (unitary element number and size), geometrical aspects (focal spot size, beam collimation), acquisition parameters (rotation angle, number of projections, rotation duration time) and reconstruction parameters like: kernel type, voxel reconstructed size and reconstruction algorithm. Unlike other studies,[4] the phantom developed for this study does allow quantitative and qualitative measurements of spatial resolution in the axial plane and also in the transaxial direction. Our results do not demonstrate the supremacy of one apparatus over the other in terms of spatial resolution. In general, our results, coming from the phantom or the dry skull, demonstrate that small-voxel size protocols (1, 2, 5 and 6) provide equivalent results on the two apparatus (Table 5) (Figures 2, 3, 5 and 6).

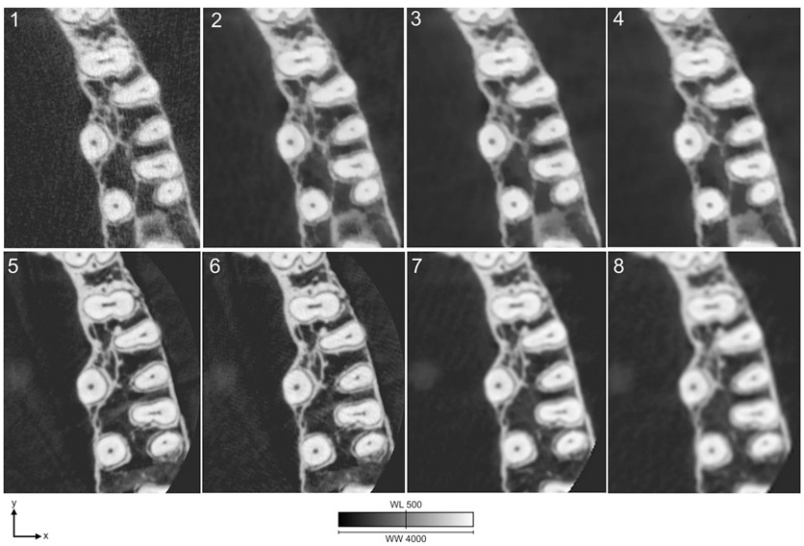

Figure 5 Axial slice at the same position of the dental region obtained with each protocol (1 to 8; Table 1) on the human dry skull; window level (WL): 500; window width (WW): 4000.

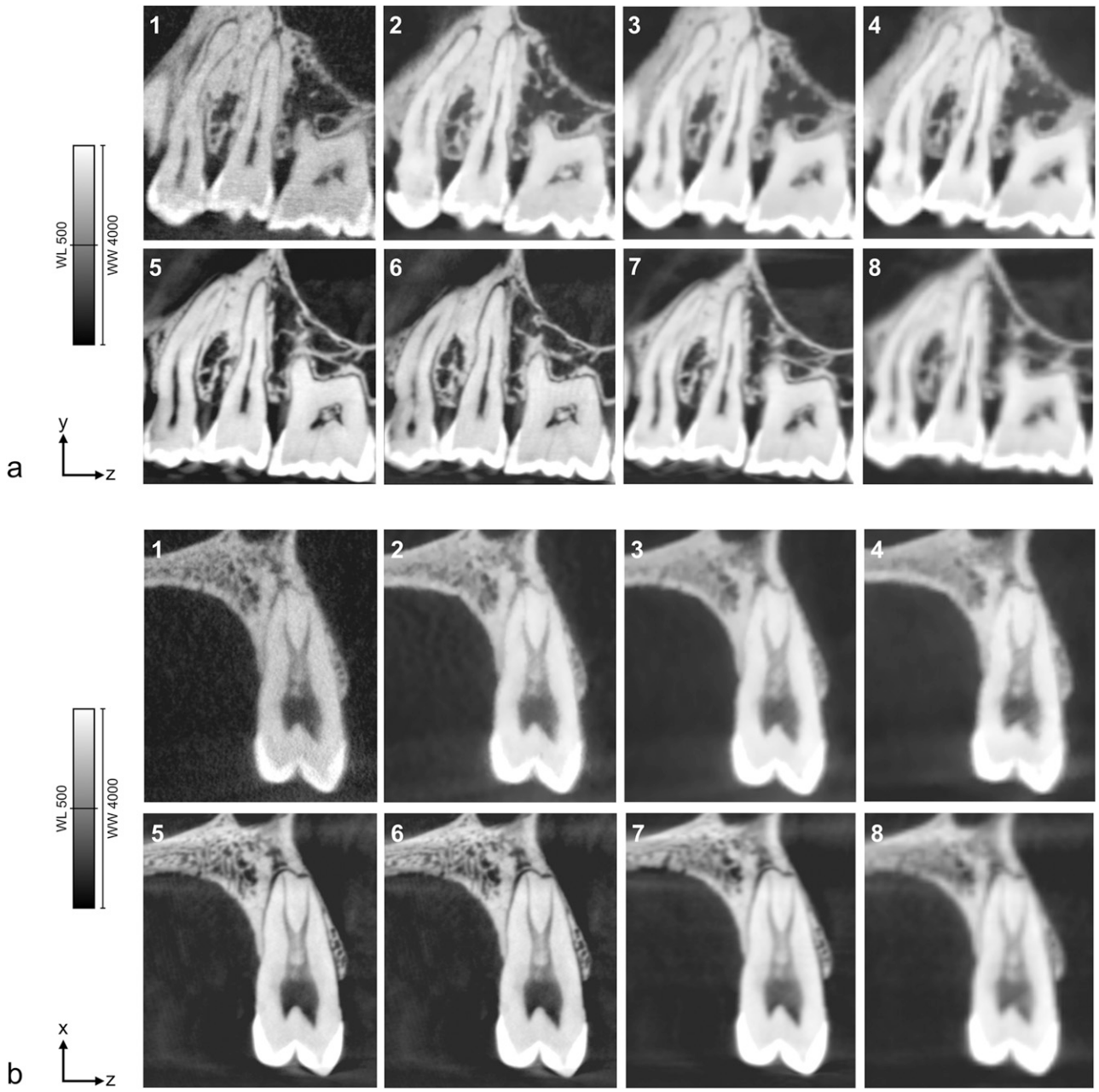

Figure 6 Sagittal (a) and coronal (b) slices at the same position of the dental region obtained with each protocol (1–8; Table 1) on the human dry skull. Window level (WL): 500; window width (WW): 4000.

Image homogeneity and geometric accuracy

The CBCT offers a large *z*-direction acquisition field by using a flat-panel detector. This geometry presents the advantage of acquiring a whole volume in a single rotation. However, it is more sensitive to scattered radiation, which has an impact on image homogeneity.[3,4,9,10] Even if the size of the phantoms used (Figure 1) allows including different patterns (*e.g.* resolution and linearity patterns) in small FOVs, their size limits scattering effects, but allows assessing intrinsic performances. The use of a dry human skull follows this statement too. In terms of linearity, all systems present similar and robust results (Table 5). In terms of homogeneity, we notice that the Planmeca system is less homogeneous than the Newtom™ system (Table 4 and Figures 3 and 5–7). The acquisition rotation angle was equal to 360° for the Newtom™ system and 200° for the Planmeca (Table 1), which could, in part, explain the homogeneity differences in favour of the Newtom™ system (Table 6 and Figure 4). Other points could explain such differences (*e.g.* misalignment artefacts, peak tube voltage and tube current settings, algorithm and kernel used),[11] but our study did not focus on this aspect.

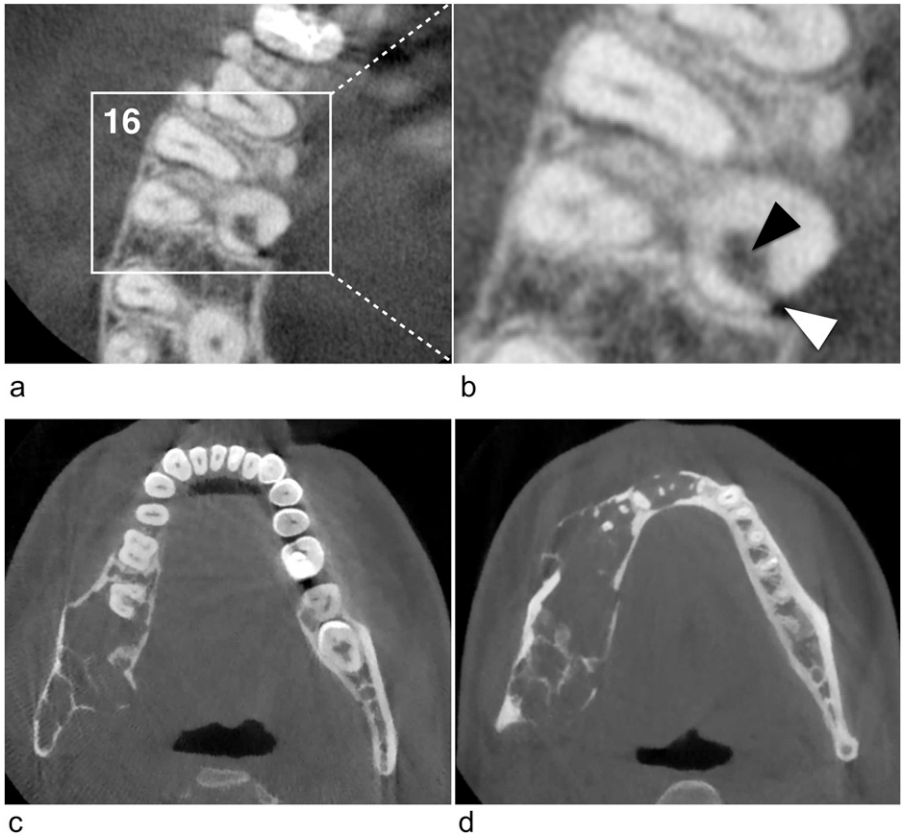

Figure 7 (a, b) Small field-of-view (FOV) CBCT axial slice (Acquisition 5, Table 1): upper right maxillary dentition showing perforating (white arrowhead) internal resorptive defect (black arrowhead) in the palatal root of the first permanent molar. (c, d) Large FOV CBCT images (Acquisition 3, Table 1): extensive lesion from the ramus to the mandibular symphysis corresponding to an odontogenic myxoma. This expansive cyst-like well-defined mandibular radiolucent lesion is showing mixed radiolucent–radiopaque internal pattern with some characteristic straight septa.

Practical aspect

Our study is limited to the two latest models available in our university hospital. We do not discuss practical aspects such as reconstruction speed and post-processing. We note that in our clinical practice, access to two different CBCT systems is an advantage. This study allowed us to determine which protocols should be used in clinical routine. Following these results:

– We only use the Planmeca Promax CBCT for high-resolution protocols with isotropic voxels of 75- or 100-μm edge lengths [Protocols 5 and 6 (Table 1)]; Protocols 7 and 8 (Table 1) were never used. Protocols 5 and 6 are particularly suited to the exploration of small lesions; for instance: endodontic lesions[11] [Figure 7(a,b)], dental fractures or fissures and mandibular pre-surgical implant site assessment.[12] In terms

Figure 8 Axial CBCT slice with patient motion artefacts that affect image quality (a); axial CBCT slice without motion artefacts (b); and seated position limiting the risk of movement artefacts (c).

of image quality, no differences were noticed between these two protocols. Also, the Planmeca system presents the advantage of 2D imaging possibility.
– The Newtom™ CBCT VGi is essentially used with large FOV protocols, giving isotropic voxels of 250- or 300-μm edge lengths [Protocols 3 and 4 (Table 1)]. These protocols are particularly appropriate for the evaluation of extended pathologies; for instance: maxillary and/or mandibular lesion like tumours or cysts [Figure 7(c,d)], bone diseases (*e.g.* osteonecrosis, osteomyelitis), maxillary or mandibular fractures and pre-operative implant site assessment[13] in extensive maxillary and/or mandibular restoration. From a practical point of view, for small lesions, Protocol 1 (Newtom™ VGi) could be an alternative to Protocols 5 and 6 (Planmeca Promax).

In general, closer attention needs to be given to the management of patient motion artefacts in CBCT owing to rotation duration, which takes more than 20 s in all protocols (Table 1). For this reason, and especially in cases of bone trauma and patients who are restless, it is imperative to pay attention to patient positioning in terms of comfort and stability. Even if CBCT is performed with the patient in a standing position, in our daily practice, we performed CBCT in seated position, to limit the risk of movement artefacts (Figure 8).[11] Further studies could be carried out to evaluate head motion and therefore define adequate positions and supports to further reduce it.

In this study, we chose to limit our focus on image properties and did not look at radiation safety considerations. Different studies proposed exhaustive works and reviews about CBCT dosimetry.[3,14]

State of the art

CBCT is nowadays a robust technology in the field of dentomaxillary imaging. Other regions that are in a validation stage could be explored in CBCT: temporal bone, temporomandibular joint, and also musculoskeletal joints with specific systems. However, this technology is still evolving: current studies, concerning all kinds of CBCT apparatus (*e.g.* dental CBCT, C-arm CBCT, CBCT-guided radiotherapy), are trying to solve some problems such as homogeneity and to improve visualization of soft tissues and image quality by using, for instance, statistical reconstruction algorithms.[15]

Conclusions

For limited OMF volume imaging (diameter < 50 mm), the Planmeca Promax 3D system used in this study could reach equivalent performances as the Newtom™ VGi CBCT. From a practical point of view, these two devices are complementary; on one hand, the Planmeca Promax 3D is used for endodontic explorations (Protocols 5 and 6) and for 2D dental panoramix imaging and on the other hand, the Newtom™ VGi CBCT is mainly used with large FOV protocols (Protocols 3 and 4) for the evaluation of extended OMF pathologies.

References

1. Mozzo P, Procacci C, Tacconi A, Martini PT, Andreis IA. A new volumetric CT machine for dental imaging based on the cone-beam technique: preliminary results. *Eur Radiol* 1998; **8**: 1558–64. doi: http://dx.doi.org/10.1007/s003300050586
2. De Vos W, Casselman J, Swennen GR. Cone-beam computerized tomography (CBCT) imaging of the oral and maxillofacial region: a systematic review of the literature. *Int J Oral Maxillofac Surg* 2009; **38**: 609–25. doi: http://dx.doi.org/10.1016/j.ijom.2009.02.028
3. Kiljunen T, Kaasalainen T, Suomalainen A, Kortesniemi M. Dental cone beam CT: a review. *Phys Med* 2015; **31**: 844–60. doi: http://dx.doi.org/10.1016/j.ejmp.2015.09.004
4. Dillenseger JP, Matern JF, Gros CI, Bornert F, Goetz C, Le Minor JM, et al. MSCT *versus* CBCT: evaluation of high-resolution acquisition modes for dento-maxillary and skull-base imaging. *Eur Radiol* 2015; **25**: 505–15. doi: http://dx.doi.org/10.1007/s00330-014-3439-8
5. Jaszczak RJ. *U.S. Patent No. 4 499 375*. Washington, DC: U.S. Patent and Trademark Office; 1985.
6. Du LY, Umoh J, Nikolov HN, Pollmann SI, Lee TY, Holdsworth DW. A quality assurance phantom for the performance evaluation of volumetric micro-CT systems. *Phys Med Biol* 2007; **52**: 7087–108. doi: http://dx.doi.org/10.1088/0031-9155/52/23/021
7. Droege RT, Morin RL. A practical method to measure the MTF of CT scanners. *Med Phys* 1982; **9**: 758–60. doi: http://dx.doi.org/10.1118/1.595124
8. Rosset A, Spadola L, Ratib O. OsiriX: an open-source software for navigating in multidimensional DICOM images. *J Digit Imaging* 2004; **17**: 205–16. doi: http://dx.doi.org/10.1007/s10278-004-1014-6
9. Pauwels R, Beinsberger J, Stamatakis H, Tsiklakis K, Walker A, Bosmans H, et al. Comparison of spatial and contrast resolution for cone-beam computed tomography scanners. *Oral Surg Oral Med Oral Pathol Oral Radiol* 2012; **114**: 127–35. doi: http://dx.doi.org/10.1016/j.oooo.2012.01.020
10. Hofmann E, Schmid M, Sedlmair M, Banckwitz R, Hirschfelder U, Lell M. Comparative study of image quality and radiation dose of cone beam and low-dose multislice computed tomography—an in-vitro investigation. *Clin Oral Investig* 2014; **18**: 301–11. doi: http://dx.doi.org/10.1007/s00784-013-0948-9
11. Schulze R, Heil U, Gross D, Bruellmann DD, Dranischnikow E, Schwanecke U. et al. Artefacts in CBCT: a review. *Dentomaxillofac Radiol* 2011; **40**: 265–73. doi: http://dx.doi.org/10.1259/dmfr/30642039
12. Horner K, Islam M, Flygare L, Tsiklakis K, Whaites E. Basic principles for use of dental cone beam computed tomography: consensus guidelines of the European Academy of Dental and Maxillofacial Radiology. *Dentomaxillofac Radiol* 2009; **38**: 187–95. doi: http://dx.doi.org/10.1259/dmfr/74941012
13. Guerrero ME, Jacobs R, Loubele M, Schutyser F, Suetens P, van Steenberghe D. State-of-the-art on cone beam CT imaging for preoperative planning of implant placement. *Clin Oral Investig* 2006; **10**: 1–7. doi: http://dx.doi.org/10.1007/s00784-005-0031-2
14. Roberts JA, Drage NA, Davies J, Thomas DW. Effective dose from cone beam CT examinations in dentistry. *Br J Radiol* 2009; **82**: 35–40. doi: http://dx.doi.org/10.1259/bjr/31419627
15. Wang AS, Stayman JW, Otake Y, Kleinszig G, Vogt S, Gallia GL, et al. Soft-tissue imaging with C-arm cone-beam CT using statistical reconstruction. *Phys Med Biol* 2014; **59**: 1005–26. doi: http://dx.doi.org/10.1088/0031-9155/59/4/1005